

## **Bi<sub>2</sub>O<sub>3</sub> with Reduced Graphene Oxide Composite as a Supercapacitor Electrode**

Shanshan Liu, Yansu Wang\*, Zhiling Ma\*

College of Chemistry and Environmental Science, National Demonstration Center for Experimental Chemistry Education, Hebei University, Key Laboratory of Analytical Science and Technology of Hebei Province, Baoding 071002, China.

\*E-mail: [15131200232@163.com](mailto:15131200232@163.com), [mazhiling838838@163.com](mailto:mazhiling838838@163.com)

Received: 27 July 2018 / Accepted: 15 September 2018 / Published: 5 November 2018

---

The bismuth oxide/reduced graphene oxide (Bi<sub>2</sub>O<sub>3</sub>/rGO) composite was synthesized by solvothermal method at different calcination temperatures. The morphology and phase structure of the Bi<sub>2</sub>O<sub>3</sub>/rGO composite was characterized using thermogravimetric analysis (TGA), X-ray diffraction (XRD), electron microscopy (SEM), and Brunauer-Emmett-Teller (BET). Meanwhile, the electrochemical performance of the Bi<sub>2</sub>O<sub>3</sub>/rGO was obtained on the electrochemical workstation. The calcination temperature directly influenced the transformation of the precursor and the morphology and structure of the material obtained after calcination, which further affected the electrochemical properties of the material. At a calcination temperature of 350°C, Bi<sub>2</sub>O<sub>3</sub>/rGO composite has a good crystallinity, uniform dispersion and excellent electrochemical performance. The composite specific capacitance is 617.1 F·g<sup>-1</sup> in 6 M KOH by chronopotentiometry at a specific current of 1 A·g<sup>-1</sup>, and the composite also displays a low resistance. These results indicate that Bi<sub>2</sub>O<sub>3</sub>/rGO composite has great prospects for supercapacitor electrode materials.

---

**Keywords:** Bi<sub>2</sub>O<sub>3</sub>/rGO; Supercapacitor; Electrochemical properties

### **1. INTRODUCTION**

In recent years, many kinds of fossil energy have been exhausted under the mining of people day and night. At the same time, due to the technical limitations, the efficiency of fossil energy is low, which lead to energy waste and environmental problems [1]. With the continuous development of society, traditional energy will be gradually eliminated. As new energy storage and conversion devices, supercapacitors are favored by many researchers [2]. For new style energy devices, supercapacitors are received more and more attention, due to many advantages such as fast charging and discharging, high power density and so on [3]. According to the charge storage mechanism,

supercapacitors can be divided into electrical double-layer capacitors and pseudocapacitors. For electrical double-layer capacitors, the electrode materials include activated carbon and graphene. These electrode materials often show good electrical conductivity but low capacitance. For pseudocapacitors, the electrode materials include conducting polymers and metal oxides, among the metal oxides display high specific capacitance, but expensive price and poor conductivity [4,5]. Therefore, it is a challenge to design new methods to ameliorate the properties of supercapacitor electrode materials.

Graphene is one of the most intensive researched electrode materials for supercapacitors because of its high carrier mobility, large electrical conductivity, high specific surface area as well as high mechanical strength and chemical resilience. Moreover, graphene can exhibit superior energy storage performances compared with graphite, carbon nanotubes and other carbon nanostructures [6]. It has been reported that graphene displayed a high specific capacitance and excellent electrical conductivity [7~9]. In particular, Ting Liu [10] proposed a porous carbon/graphene composite, material as-prepared porous carbon/graphene composite can deliver specific capacitance of up to 340  $\text{F}\cdot\text{g}^{-1}$  at 5  $\text{mV}\cdot\text{s}^{-1}$  in 6 M KOH electrolyte and the values of  $R_{ct}$  and  $R_s$  less than 1  $\Omega$ . At present, metal oxide materials such as  $\text{MnO}_2$  [11],  $\text{Co}_3\text{O}_4$  [12],  $\text{Fe}_3\text{O}_4$  [13],  $\text{ZnO}$  [14],  $\text{CeO}_2$  [15] and  $\text{NiO}$  [16] have been widely used in electrode materials research, and these materials are used as positive electrode material for electrochemical energy storage devices. However, XueJing Ma [17] mentioned that Bi-based compounds stand a chance to become an underlying negative electrode material for electrochemical energy storage devices. Such as Sarma Biplab [18], Jiangfeng Li [19], Shixing Wang [20], Mateuse Ciszewski [21] and Yongfu Qiu[22] so on reported about  $\text{Bi}_2\text{O}_3$  compound acted as the electrode materials, which that displayed high specific capacitance characteristics. For these reasons, combining metal oxide and graphene, we can obtain electrode materials with high capacitance and low resistance.

In this work, the bismuth oxide/reduced graphene oxide ( $\text{Bi}_2\text{O}_3/\text{rGO}$ ) composite was firstly synthesized by solvothermal method at different calcination temperatures. Subsequently, the prepared material was characterized using thermogravimetric analysis (TGA), scanning X-ray diffraction (XRD), electron microscopy (SEM), and Brunauer-Emmett-Teller (BET). Finally, the electrochemical performance cyclic voltammetry (CV), galvanostatic charge/discharge (GCD) and electrochemical impedance spectroscopy (EIS) of the  $\text{Bi}_2\text{O}_3/\text{rGO}$  electrode were tested on the electrochemical workstation.

## 2. EXPERIMENTAL

### 2.1. Materials

All chemicals used in the present work were of analytical grade and were used without further purification, and distilled water was used throughout the experiments.  $\text{Bi}(\text{NO}_3)_3\cdot 5\text{H}_2\text{O}$ , N,N-dimethylformamide (DMF), nickel foam and conductive carbon black were purchased from Tianjin Ke Miou Chemical Reagent Co., Ltd. Polytetrafluoroethylene (PTFE, the mass fraction is 60%) solution

was brought from Aladdin. Potassium hydroxide (KOH) was purchased from Tianjin Fu Chen Chemical Co., Ltd.

## 2.2. Synthesis of $\text{Bi}_2\text{O}_3/\text{rGO}$ composite

Graphite oxide (GO) was synthesized from graphite powder by Hummers method.  $\text{Bi}_2\text{O}_3/\text{rGO}$  composite was prepared as follows: 100 mg of graphite oxide and 104 mg of  $\text{Bi}(\text{NO}_3)_3 \cdot 5\text{H}_2\text{O}$  were dispersed in 45 mL of DMF with ultrasonication for 60 min (the theoretical mass ratio of GO and  $\text{Bi}_2\text{O}_3$  is 1:1). Then, the mixture was placed in a Teflon-lined autoclave and reacted at 180°C for 12 hours. After cooling to room temperature, the as-prepared product was isolated by filtering, washed three times with water and ethanol, respectively, and finally dried in a vacuum oven at 60°C for 24 hours. Under air atmosphere, the dried product was heated in a tube furnace at 250°C, 300°C, 350°C for 4 h to get the final  $\text{Bi}_2\text{O}_3/\text{rGO}$  composites, which were denoted sample A, B, C, respectively.

## 2.3. Materials characterization

The X-ray powder diffraction of the samples were conducted using a Bruker D8 Advance X-ray diffractometer with Cu  $\text{K}\alpha$  radiation (40 kV, 40 mA), the scanning range was fixed at 5~80° at a scanning rate of 5°·min<sup>-1</sup>. The morphology of the prepared composite was characterized by SEM. The specific surface area and pore structure of the samples were determined by BET. Thermogravimetric analysis (TGA) was carried out in air atmosphere and a temperature range of 30-800°C.

## 2.4. Electrochemical performance

All tests of electrochemical properties were performed in 6 M KOH aqueous electrolyte using a Gamry electrochemical workstation. The working electrodes were prepared as follows: 80%  $\text{Bi}_2\text{O}_3/\text{rGO}$ , 15% conductive carbon black, 5% PTFE (the mass fraction is 10%), and a small amount of ethanol were uniformly mixed. Then the mixture was uniformly coated on a foamed nickel with an area of 1 cm<sup>2</sup>, and pressed into a sheet at a pressure of 10 MPa and dried at 60°C for 12 hours. Prior to testing, the working electrode was immersed in 6 M KOH for 24 hours at room temperature in a vacuum environment.

Cyclic voltammetry (CV) was carried out in the potential window range of -1.0 to -0.2 V at different scan rates. The galvanostatic charge/discharge (GDC) test was carried out at various current densities over a voltage window from -1.0 to -0.2 V. Electrochemical impedance spectroscopy (EIS) was performed in a frequency range from 0.01 Hz to 100 kHz. The specific capacitance is calculated as follows:  $C_s = I\Delta t / m\Delta V$  ( I (A) -- discharge current;  $\Delta t$  (s) -- discharge time; m (g) -- weight of the active material composite;  $\Delta V$  (V) -- potential drop ).

### 3. RESULTS AND DISCUSSION

#### 3.1. Structural and morphological

To understand the thermal degradation process of as-prepared  $\text{Bi}_2\text{O}_3/\text{rGO}$  composite, TG analysis was carried out in an air atmosphere of  $30^\circ\text{C}$  to  $800^\circ\text{C}$ . Figure 1 shows the TGA and DTG results of  $\text{Bi}_2\text{O}_3/\text{rGO}$  composite. For  $\text{Bi}_2\text{O}_3/\text{rGO}$  composite, there is 5% weight loss around  $375^\circ\text{C}$ , and after  $375^\circ\text{C}$  the mass loss dramatically increases. The large weight is due to the degradation of rGO [23]. The calcination temperature is up to  $350^\circ\text{C}$ , otherwise there will be no rGO in the composite. Therefore, the calcination temperature selected for the experiment was  $250^\circ\text{C}$ ,  $300^\circ\text{C}$ , and  $350^\circ\text{C}$ . Above  $450^\circ\text{C}$ , there is no obvious weight loss, illustrating the rGO was all removed. Figure 1 indicates the composite contains about 47.57%  $\text{Bi}_2\text{O}_3$ , which is close to the theoretical value of 50%.

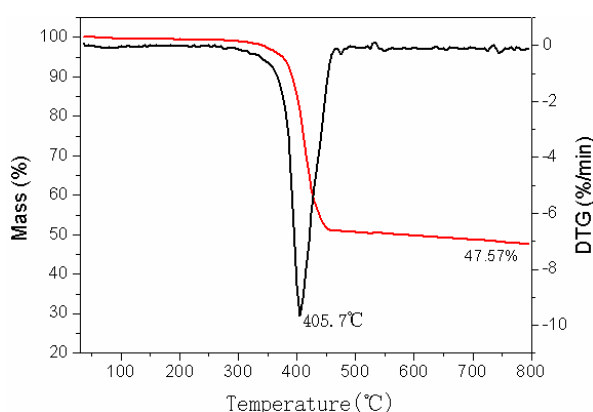
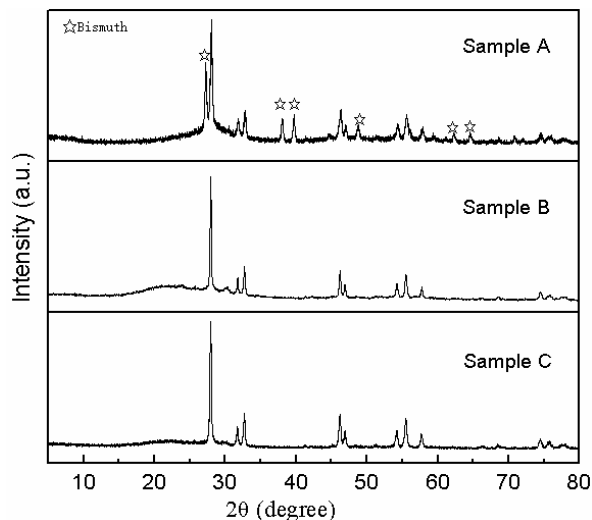


**Figure 1.** TGA and DTG of  $\text{Bi}_2\text{O}_3/\text{rGO}$  composite.

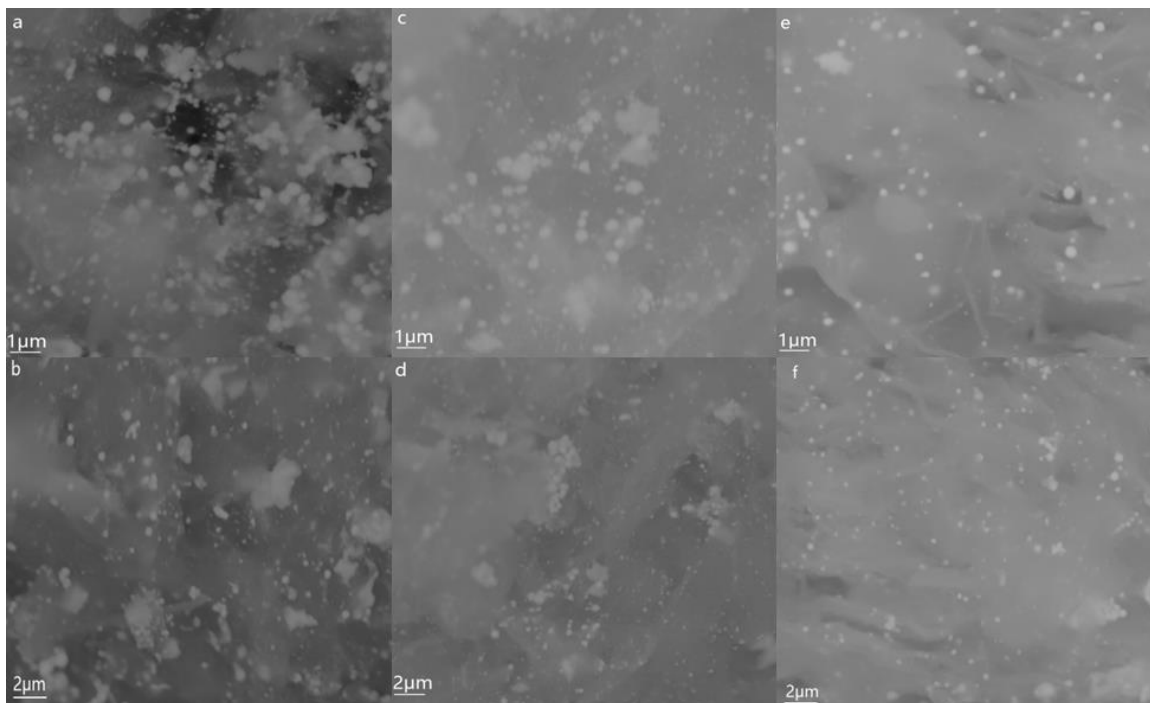
Figure 2 shows the XRD patterns of sample A, B, C. The diffraction peaks of the  $\text{Bi}_2\text{O}_3/\text{rGO}$  composite at  $2\theta$  values  $27.9^\circ$ ,  $31.7^\circ$ ,  $32.7^\circ$ ,  $46.2^\circ$ ,  $46.9^\circ$ ,  $54.2^\circ$ ,  $55.5^\circ$ ,  $57.8^\circ$  and  $74.5^\circ$  can correspond well to the bismuth oxide (JCPD No.27-0050). However, for the XRD pattern of sample A, it's clearly seen that the diffraction peak at around  $2\theta=27.1^\circ$ ,  $38^\circ$ ,  $39.6^\circ$ ,  $48.7^\circ$ ,  $62.2^\circ$ ,  $64.5^\circ$  are in agreement with the bismuth (JCPD No.44-1246), demonstrating that the precursor prepared is not completely converted to  $\text{Bi}_2\text{O}_3$  at  $250^\circ\text{C}$ . For the XRD patterns of sample B and C, it can be seen that the diffraction peaks of  $\text{Bi}_2\text{O}_3$ , all the diffraction peaks of  $\text{Bi}_2\text{O}_3$  can be observed and there are no diffraction peaks of Bi and graphene, which indicates that composites is successfully synthesized. In addition, the diffraction peak of sample C is sharper, we can conclude that the crystal structure of  $\text{Bi}_2\text{O}_3$  is more regular.

Figure 3 shows the SEM images of as-synthesized  $\text{Bi}_2\text{O}_3/\text{rGO}$  materials at different calcination temperatures. It can be observed that  $\text{Bi}_2\text{O}_3$  particles agglomerate together to form the SEM of sample A (figure 3a, b) and sample B (figure 3c, d). In contrast,  $\text{Bi}_2\text{O}_3$  particles are well distributed on the graphene sheet to form the SEM of sample C (figure 3e, f), and the wrinkles of the graphene are also clearly seen. Therefore, calcination temperature affects the morphology of the material, and as the calcination temperature increases, the degree of agglomeration gradually decreases. Most importantly,

the wrinkled graphene can effectively prevent agglomeration among graphene and increase the wetted area between the electrode and the electrolyte [24].



**Figure 2.** XRD spectrums of samples



**Figure 3.** (a, b) the SEM image of Sample A; (c, d) the SEM image of Sample B; (e, f) the SEM image of Sample C.

The specific surface area and pore structure of the  $\text{Bi}_2\text{O}_3/\text{rGO}$  composites were studied by the nitrogen adsorption/desorption method. The  $\text{N}_2$  isotherms and pore-size distributions of the sample C are shown in Figure 4. The as-synthesized  $\text{Bi}_2\text{O}_3/\text{rGO}$  is found to have a specific surface area of  $27.3 \text{ m}^2 \text{ g}^{-1}$  and a average pore-size diameters of 25 nm, so it belongs to a mesoporous material. It has been

reported that mesoporous with pore sizes between 2 and 50 nm can effectively improve the infiltration of materials in electrolyte [25].

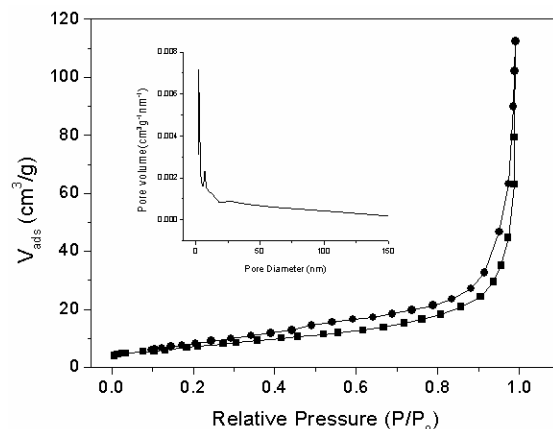
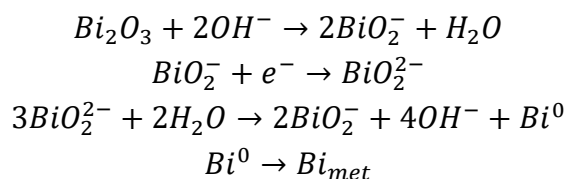


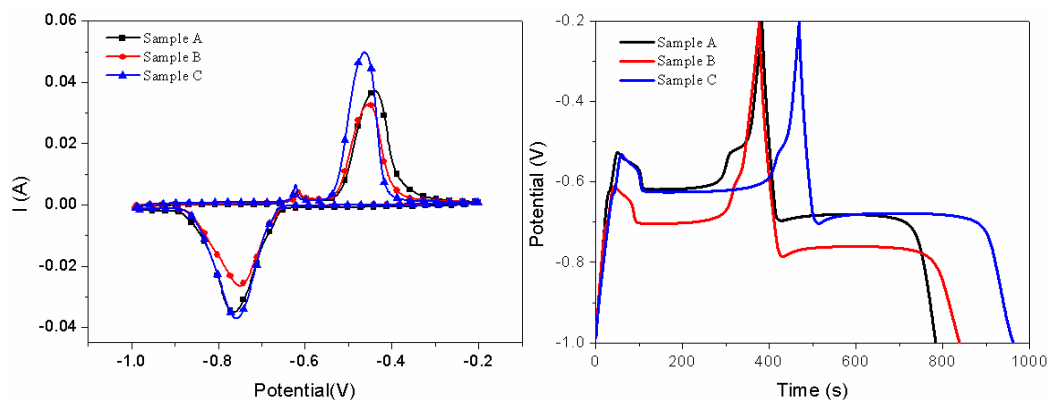
**Figure 4.** Nitrogen adsorption-desorption isotherms of Sample C

### 3.2 Electrochemical properties

Cyclic voltammetry (CV) measurements were used to investigate the electrochemical performance of the  $\text{Bi}_2\text{O}_3/\text{rGO}$  in 6 M KOH aqueous electrolyte at room temperature. Figure 5a shows the CV curves of sample A, B, C recorded at a sweep rate of  $5 \text{ mV s}^{-1}$ , and a couple of redox peaks can be observed clearly in the CV curves, which implying the typical pseudocapacitive behaviors for  $\text{Bi}_2\text{O}_3$  electrodes, and the reaction process is as follows [26]:

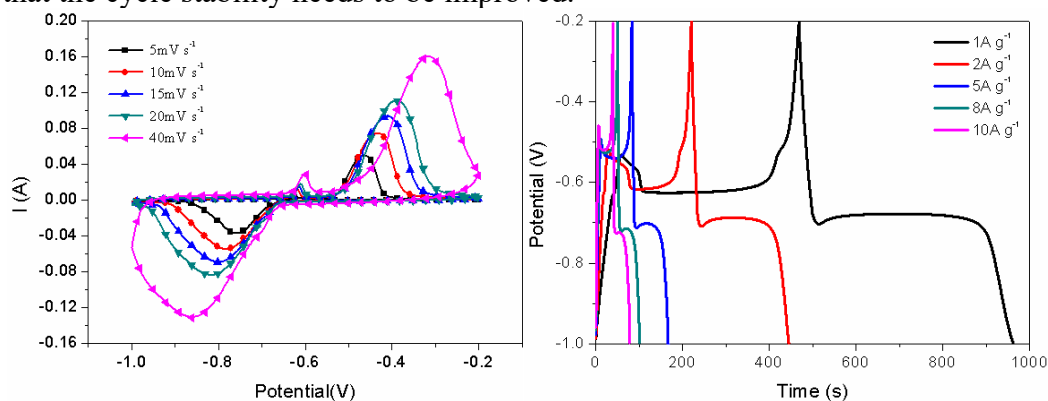


where  $\text{Bi}^0$  is active atoms,  $\text{Bi}_{\text{met}}$  is the metal bismuth. The small oxidation peak at around  $-0.6\text{V}$  is also noticed in reports [19,22]. The integrated area of the sample C is bigger than that of sample A and B, suggesting that sample C has a higher specific capacitance [27]. Figure 5b exhibits the galvanostatic charge/discharge curves of the  $\text{Bi}_2\text{O}_3/\text{rGO}$  samples at a current density of  $1 \text{ A}\cdot\text{g}^{-1}$ . According to the calculation equation of the specific capacitance mentioned above, at the same current density, the specific capacitance of the electrode increases with an increase in the discharge time. As depicted figure 5b, the specific capacitance of sample C is largest because it has more regular crystal structure and better uniform degree. This is consistent with the result of CV tests. The specific capacitance of Sample C is  $617.13 \text{ F}\cdot\text{g}^{-1}$  at  $1 \text{ A}\cdot\text{g}^{-1}$  according to the equation.



**Figure 5.** (a) cyclic voltammetry curves of samples at scan rate  $5 \text{ mV}\cdot\text{s}^{-1}$ ; (b) galvanostatic charge/discharge curves of the samples at a current density of  $1 \text{ A}\cdot\text{g}^{-1}$

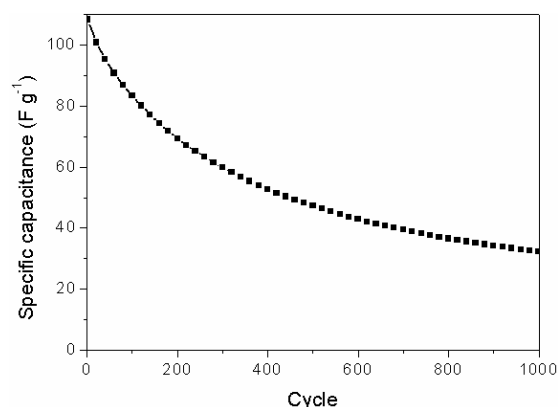
Figure 6a shows the CV curves of sample C at different scan rates. It can be seen that CVs of sample C retain a similar shape even at high sweep rate, indicating an excellent capacitance behavior and the fast diffusion of electrolyte ions into the composite [23]. The galvanostatic charge/discharge curves were measured at different current densities, ranging from 1 to  $10 \text{ A}\cdot\text{g}^{-1}$  (Figure 6b), and the horizontal charge/discharged plat-forms exhibit the pseudocapacitance of the  $\text{Bi}_2\text{O}_3$ . The specific capacitances of the electrode decreases with the increase of the current densities. When the current density is  $1 \text{ A}\cdot\text{g}^{-1}$ , the specific capacitance is  $617.13 \text{ F}\cdot\text{g}^{-1}$ ; when the current density increased to  $10 \text{ A}\cdot\text{g}^{-1}$ , the specific capacitance reduced to  $490.6 \text{ F}\cdot\text{g}^{-1}$ , and the capacitance retention rate is 79.5%. In addition, compared with the present reports [18-22] on bismuth-based oxide as electrode materials (Table 1), as-prepared composite has a larger specific capacitance and lower resistance. As the current density increase, the gradually decrease of the specific capacitance is ascribed to the fast-transmitting electrons, as it does not have sufficient time to contact the surface of the electrode material and cannot completely react [28]. Figure 7 shows the cycling stability of the sample C by circulating charging and discharging at a current density of  $5 \text{ A}\cdot\text{g}^{-1}$ . The capacitance retention is 30% after 1000 cycles, which indicating that the cycle stability needs to be improved.



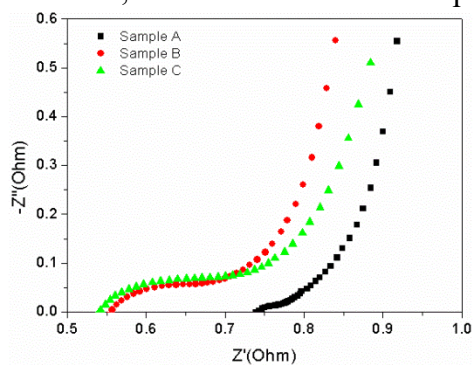
**Figure 6.** (a) cyclic voltammograms curves of sample C at different scan rates; (b) galvanostatic charge/discharge curves sample C at different current densities

**Table 1.** The specific capacitance of supercapacitance bismuth-based oxide in papers

Material	Capacitance	Current density	Rs / Rct	Electrolyte	Ref
T-NT/Bi <sub>2</sub> O <sub>3</sub>	430 mF·cm <sup>-2</sup>	5 mA·cm <sup>-2</sup>	-	1 M KOH	[18]
Bi <sub>2</sub> O <sub>3</sub> -AC	466 F·g <sup>-1</sup>	1 A·g <sup>-1</sup>	2.16 Ω / 0.24 Ω	6 M KOH	[19]
AC- Bi <sub>2</sub> O <sub>3</sub>	332.6 F·g <sup>-1</sup>	1 A·g <sup>-1</sup>	0.7 Ω / 0.44 Ω	6 M KOH	[20]
rGO- Bi <sub>2</sub> O <sub>3</sub>	94 F·g <sup>-1</sup>	0.2 A·g <sup>-1</sup>	-	6 M KOH	[21]
Bi <sub>2</sub> O <sub>3</sub> nanowires	691.3 F·g <sup>-1</sup>	2 A·g <sup>-1</sup>	1.23 Ω / 1.0 Ω	6 M KOH	[22]

**Figure 7.** Galvanostatic charge/discharge cycles of sample C at a current density of 5 A g<sup>-1</sup>

Electrochemical impedance spectroscopy (EIS) was conducted to evaluate the electrochemical conductivity behaviors of three samples electrodes. Figure 8 shows the typical Nyquist plots of the samples electrodes at open circuit potential in the frequency range from 0.01 Hz to 100 kHz with amplitude of 5 mV. The Nyquist plots present similar shapes with a depressed semicircle at high frequency region and a straight line at low frequency region. At high frequencies, the intercept of the Nyquist curve on the real axis represents the solution resistance (Rs), including the intrinsic resistance of active materials, ionic resistance of electrolyte, and contact resistance at the active materials/current collector interface, while the semicircle corresponds to the charge transfer resistance (Rct) [29]. From figure 8, it can be seen that the values of the sample C Rs and Rct are 0.54 Ω and 0.2 Ω, respectively. This shows that Bi<sub>2</sub>O<sub>3</sub>/rGO is a low resistance material, which is beneficial to electronic transmission. The straight line at low frequencies region corresponds to the diffusive resistance of the electrolyte ion [30]. The diffusive resistance of the three samples is close, but the solution resistance and charge transfer resistance of sample C are smaller, which show that the sample C has excellent conductivity.

**Figure 8.** Nyquist plot of the samples

#### 4. CONCLUSIONS

Bi<sub>2</sub>O<sub>3</sub>/rGO composite was successfully synthesized via a facile solvothermal method. At a calcination temperature of 350°C, Bi<sub>2</sub>O<sub>3</sub>/rGO composite electrode exhibits highest capacitive performances with perfect crystallinity. The specific capacitance is 617.13 F·g<sup>-1</sup> at current density 1 A·g<sup>-1</sup>. As current density is increased to 10 A·g<sup>-1</sup>, the capacitance retention rate is 79.5%. The capacitance retention of 30% after 1000 cycles at 5 A·g<sup>-1</sup>, and the internal resistance of the material is less. Therefore, the prepared reduced graphene oxide/bismuth oxide is an ideal material for supercapacitors.

#### ACKNOWLEDGEMENTS

This work was supported by the Natural Science Foundation of Hebei Province (Nos. B2014201024) funding

#### References

1. N. Choudhary, C. Li, J. Moore, N. Nagaiah, L. Zhai, Y. Jung, J. Thomas, *Adv. Mater*, 29 (2017).
2. S. D. Lee, H. S. Lee, J. Y. Kim, J. Jeong, Y. H. Kahng, *Mater. Res. Express*, 4 (2017) 085604.
3. J. M. Jiang, Y. D. Zhang, P. Nie, G. Y. Xu, M.Y. Shi, J. Wang, Y. T. Wu, R. R. Fu, H. Dou, X. G. Zhang, *Adv. Sustainable Sys.*, 2 (2018).
4. Y. Y. Wang, X. Xiao, H. G. Xue, H. Pang, *Chemistryselect*, 3 (2018) 550.
5. D. Y. Su, J. Ma, M. Y. Huang, F. Liu, T. Z. Chen, C. Liu, H. J. Ni. *IOP Conf. Series: Materials Science and Engineering*, 207 (2017) 012087.
6. J. Ph. Mensing, C. Poochai, S. Kerdpocha, C. Sriprachuabwong, A. Wisitsoraat, A. Tuantranont, *Adv. Nat. Sci. : Nanosci. Nanotechnolo.* , 8 (2017) 033001.
7. Y. H. Kwon, S. Kumar, J. Bae, Y. Seo. *Nanotechnology*, 29 (2018) 195404.
8. S. N. Alam, N. Sharma, L. Kumar, *Graphene*, 6 (2017) 1.
9. S. Natarajan, S. Rao Ede, H. C. Bajaj, S. Kundu, *Colloids and Surfaces A*, 543 (2018) 98.
10. T. Liu, X. S. Zhang, K. Liu, Y. Y. Liu, M. J. Liu, W. Y. Wu, Y. Gu, R. J. Zhang, *Nanotechnology*, 29 (2018) 095401.
11. M. Yang, D. S. Kim, S. B. Hong, J. W. Sim, J. Kim, S. S. Kim, B. G. Choi, *Langmuir*, 33 (2017) 5140.
12. T. T. Jiang, S. Y. Yang, Z. M. Bai, P. Dai, X. X. Yu, M. Z. Wu, H. B. Hu, *Nanotechnology*, (2018).
13. X. D. Huang, B. Sun, S. Q. Chen, G. X. Wang, *Chem. Asian J.* , 9 (2014) 206.
14. A. Darari, I. S. Hakim, Priyono, A. Subagio, Pardoyo, A. Subhan, *Journal of Physics: Conf. Series*, 877 (2017) 012006.
15. Maheswari, Nallappan, M. Gopalan, D. Trans, *Dalton Trans*, 45 (2016) 14352.
16. R. S. Kate, S. A. Khalate, R. J. Deokate, *Journal of Alloys and Compounds*, 734 (2018) 89.
17. X. J. Ma, W. B. Zhang, L. B. Kong, *Electrochimica Acta.* , 192 (2016) 45.
18. B. Sarma, A. L. Jurovitzki, Y. R. Smith, S. K. Mohanty, M. Misra. *ACS Appl. Mater. Interfaces*, 5 (2013) 1688.
19. J. F. Li, Q. S. Wu, G. T. Zan. *Eur. J. Inorg. Chem.* , 2015 (2015) 5751.
20. S. X. Wang, C. C. Jin. *Journal of Alloys and Compound*, 615 (2014) 12.
21. Ma. Ciszewski, A.j Mianowski, P. Szatkowski, G. Nawrat, J. Adamek. *Ionics*, 21 (2015) 557.
22. Y. F. Qiu, H. B. Fan, X. Y. Chang, H. F. Dang, Q. Luo, Z. Y. Cheng. *Applied Surface Science*, 434 (2018)16.
23. H. W. Wang, Z. G. Hu, Y. Q. Chang, Y. L. Chen, Z. Q. Lei, Z. Y. Zhang, Y. Y. Yang. *Electrochimica*

- Acta.* , 55 (2010) 8974.
24. J. Yan, J. P. Liu, Z. J. Fan, T. Wei, L. J. Zhang. *Carbon*, 50 (2012) 2179.
25. G. Gryglewicz, E. Lorenc-Grabowska, G. Lota, E. Frackowiak. *Electrochimica Acta.* , 50 (2005) 1197.
26. V. Vivier, A. Regis, G. Sagon , J. Y. Nedelec L.T. Yu, C. Cachet-Vivier. *Electrochimica Acta.* , 46 (2001) 907.
27. M. B. Zheng, X. Xiao, L.L. Li, P. Gu, X. Dai, H. Tang, Q. Hu, H. G. Xue, H. Pang. *Sci China Mater*, 61 (2018) 185.
28. Y. C. Zhang, H. Yang, W. P. Wang, H. M. Zhang, R. S. Li, X. X. Wang, R. C. Yu. *Journal of Alloys and Compounds*, 684 (2016) 707.
29. H. J. Zheng, G. Yang, S. M. Chen, Y. Jia. *ChemElectroChem*, 4 (2017) 577.
30. D. Y. Qu, L. L. Wang, D. Zheng, L. Xiao, B. H. Deng, D. Y. Qu. *An Asymmetric Journal of Power Sources*, 269 (2014) 129.

© 2018 The Authors. Published by ESG ([www.electrochemsci.org](http://www.electrochemsci.org)). This article is an open access article distributed under the terms and conditions of the Creative Commons Attribution license (<http://creativecommons.org/licenses/by/4.0/>).